

# Mesoscale simulations of surfactant dissolution and mesophase formation

P. Prinsen,<sup>1,2</sup> P. B. Warren,<sup>1</sup> and M. A. J. Michels<sup>2</sup>

<sup>1</sup>*Unilever Research and Development Port Sunlight,  
Bebington, Wirral, CH63 3JW, United Kingdom*

<sup>2</sup>*Department of Applied Physics, Eindhoven University of Technology,  
P.O. Box 513, 5600 MB Eindhoven, The Netherlands.*

(Dated: 21 April 2002 — PREPRINT)

The evolution of the contact zone between pure surfactant and solvent has been studied by mesoscale simulation. It is found that mesophase formation becomes diffusion controlled and follows the equilibrium phase diagram adiabatically almost as soon as individual mesophases can be identified, corresponding to times in real systems of order  $10 \mu\text{s}$ .

When pure surfactant comes into contact with water, mesophases appear at the interface. This is an important process not only for the practical use of surfactants, but also from the point of view of fundamental surfactant phase science. Indeed, contact ‘flooding’ or penetration scan experiments can yield quantitative information on mesophases as a function of composition [1]. The phenomenon is invariably *diffusion controlled* in the sense that the widths of the mesophases follow  $t^{1/2}$  growth laws, and *adiabatic* in the sense that the local composition determines the mesophase boundaries according to the equilibrium phase diagram [2, 3, 4]. But penetration scan experiments are restricted to observation times of minutes to hours: what happens on time scales shorter than this? How early does diffusion control set in, and how soon can one expect the mesophase boundaries to track the local composition adiabatically? Such questions are not just of scientific interest since time scales of seconds or less are important in modern processing and the everyday use of surfactants, for instance determining how rapidly washing powder dissolves. Experimentally, this regime is very difficult to access because of the short time scales and the relatively small amounts of mesophase involved. To probe these questions therefore, we have therefore undertaken novel mesoscale simulations of surfactant dissolution. We find adiabatic diffusion control is established remarkably rapidly in our model, on time scales in which only a few repeat units of the growing mesophases have appeared, corresponding to times in the real systems of order  $10 \mu\text{s}$ .

The model we have used is a ‘minimalist’ particle-based model of a binary surfactant / water mixture, based on the dissipative particle dynamics (DPD) method [5, 6]. In DPD, the particles are soft spheres, interacting with pairwise soft potentials of the form  $U = \frac{1}{2}A(1 - r/r_c)^2$  ( $r < r_c$ ) where  $r$  is the particle separation,  $r_c$  is the range of the interaction, and  $A$  the amplitude. In the model we have three species of particles: A, B and C. The A and B particles are bound together in pairs as dimers with a fixed separation  $r_d$ , and represent the surfactants. The C particles are monomers representing the solvent (water). The different species

are distinguished by their interaction amplitudes, and the trick is to find a set of amplitudes which recover suitable phase behaviour. Following earlier work [6], we use  $A_{AA} = A_{BB} = A_{CC} = 25$ ,  $A_{AB} = 30$ ,  $A_{AC} = 0$ ,  $A_{BC} = 50$  and  $r_d = 0.5$  which gives phase diagram features lying in a convenient temperature range around  $k_B T \sim 1$  (we fix units by choosing  $m = r_c = 1$  where  $m$  is the mass of the particles).

Fig. 1 shows the phase diagram as a function of dimer concentration and  $k_B T$ , at an overall density  $\rho = (2N_{AB} + N_C)/V = 6$ , where dimer concentration is defined to be the mole fraction of particles in dimers:  $c = 2N_{AB}/(2N_{AB} + N_C)$ . Similar to many real systems [7], micellar ( $L_1$ ), hexagonal ( $H_1$ ) and lamellar ( $L_\alpha$ ) phases are found in order of increasing dimer concentration, and the interactions are chosen so that on the pure dimer side there is an isotropic fluid ( $L_2$ ) phase. The fact that a certain amount of solvent is needed to induce the  $L_\alpha$  phase reflects the real behaviour of many nonionic surfactants, and is crucial to the contact simulations below. We did not find any cubic phases, although these are not always present in real systems (an extensive study of lattice models by Larson [8] suggests that cubic phases could be engineered to appear particularly if the DPD model is elaborated beyond dimers). Also, we caution that  $k_B T$  in the model is not easily mapped onto a real temperature. Despite these deficiencies, it is nevertheless remarkable that such a simple model reproduces the main features of the phase diagram common to a large number of surfactants.

To simulate surfactant dissolution and mesophase formation with this model is now very simple. We take two simulation boxes, one containing an equilibrated fluid of pure dimers and the other containing equilibrated solvent particles. We place them next to each other and allow the dimers and solvent particles to interdiffuse. Just as in the real systems, mesophases start to appear at the interface over time. Here we report results for the  $k_B T = 1$  isotherm, although the  $k_B T = 0.5$  isotherm was also studied with similar results. We consider simulation boxes of size  $10^2 \times 100$ , with the concentration gradient along the long axis. Fig. 1 shows some representative

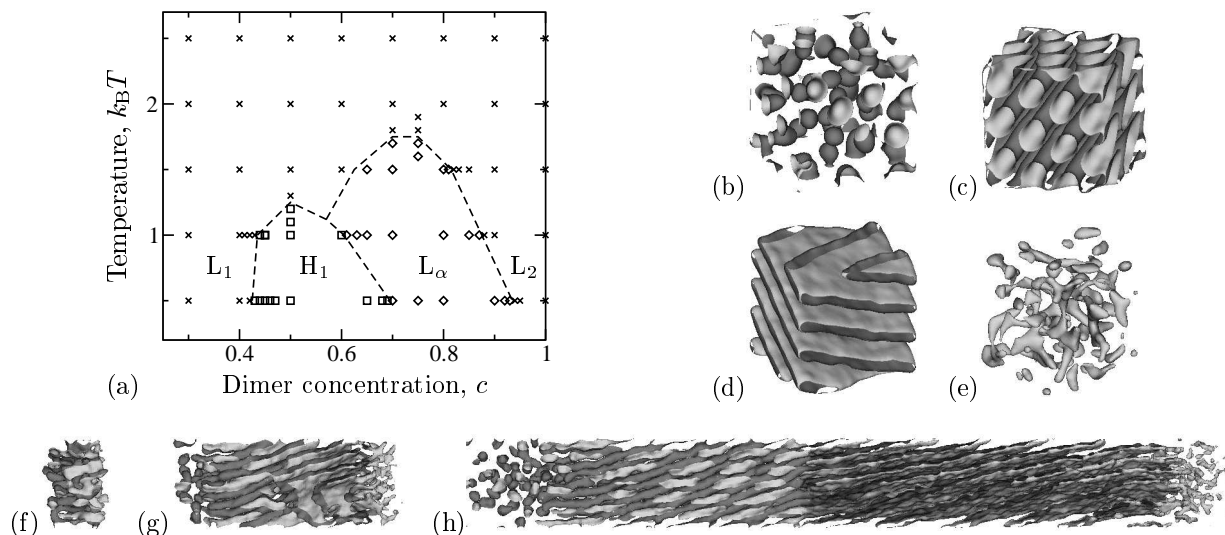


FIG. 1: (a) Phase diagram for dimer / solvent model in  $(c, k_B T)$  plane showing points where we find isotropic, hexagonal and lamellar phases (crosses, squares and diamonds respectively). The lines are a guide to the eye. (b)–(e) Isosurfaces ( $\rho_C = 1.3$ ) for equilibrium phases along  $k_B T = 1$  isotherm, at  $c = 0.3, 0.6, 0.7$  and  $0.9$  respectively. (f)–(h) Isosurfaces showing snapshots of surfactant dissolution simulations, at elapsed times  $t = 12, 120$  and  $1200$  DPD time units from initial contact.

simulation snapshots.

Whilst this is straightforward, there are a couple of technical points to be considered. Firstly it is important to adjust the densities in the two boxes so that the pressures are equal. From separate simulations, we determined the equation of state for the pure components, and found that densities  $\rho = 6.124$  and  $5.896$  for the solvent and dimers respectively give a common pressure  $p \approx 100$ . These densities are within  $\approx 2\%$  of the density  $\rho = 6$  used to construct the phase diagram in Fig. 1, which obviates the need to consider constant pressure simulations. The pressure matching is important though because it suppresses sound waves which would spoil the subsequent analysis. Secondly, if we were to use conventional periodic boundary conditions, there would be an unwanted second interface in the system. We eliminate this by bounding the simulation box in the long direction by hard reflecting walls, supplemented by short-range soft repulsive potentials of the form  $U = \frac{1}{2}A_{\text{wall}}(1 - z/r_c)^2$  ( $z < r_c$ ), where  $z$  is the distance from the hard wall. The soft repulsive force suppresses density oscillations which would otherwise arise due to the abrupt termination of the particle density. We find empirically  $A_{\text{wall}} = 25$  gives a smoothly vanishing density. Periodic boundary conditions are retained in the other two directions.

Now we turn to an objective analysis of the simulations to determine the growth laws. This is done by introducing a local order parameter which can distinguish between mesophases as a function of distance normal to the original contact plane. Although we examined various possibilities such as the use of Minkowski functionals [10], an approach which works well in practice is moti-

TABLE I: Relationship between the ordered eigenvalues  $\mu_i$  of the second moment  $\mathbf{M}$  of the isosurface normal distribution  $p(\mathbf{n})$ , the nature of  $p(\mathbf{n})$ , the expected isosurface geometry, and the expected mesophase; based on Mardia [9].

Eigenvalues of $\mathbf{M}$	$p(\mathbf{n})$	Isosurface	Mesophase
$\mu_1 \approx \mu_2 \approx \mu_3 \approx 1/3$	random	spheres/blobs	$L_1$ or $L_2$
$\mu_1 \approx 0, \mu_2 \approx \mu_3 \approx 1/2$	planar	cylinders	$H_1$
$\mu_1 \approx \mu_2 \approx 0, \mu_3 \approx 1$	axial	planes	$L_\alpha$

vated by the  $\rho_C = 1.3$  isosurfaces shown in Fig. 1. The different mesophases are clearly distinguishable to the eye because the isosurface is predominantly spherical, cylindrical, planar, or fragmented, for the  $L_1, H_1, L_\alpha$  and  $L_2$  phases respectively. This geometric insight can be made quantitative by constructing the second moment of the isosurface normal distribution  $p(\mathbf{n})$ , namely the symmetric tensor  $\mathbf{M} = \int \mathbf{n}\mathbf{n} p(\mathbf{n}) d\mathbf{n}$  [11]. The local geometric nature of the isosurface and hence the underlying mesophase is reflected in the eigenvalues  $\mu_i$  of  $\mathbf{M}$  as laid out in Table I. If these eigenvalues are ranked in order of increasing size, we determined after some trials that a slice can be classified as  $H_1$  if  $\mu_1 < 0.05$  and  $\mu_{2,3} > 0.3$ , or  $L_\alpha$  if  $\mu_1 < 0.05$  and  $\mu_2 < 0.15$  (note  $\sum_{i=1}^3 \mu_i = 1$ ).

For the present study, we divide the simulation box into slices of thickness  $0.25 r_c$  parallel to the original contact plane and determine the eigenvalues of  $\mathbf{M}$  for each slice. Fig. 2(a) gives a representative example, showing that the various mesophases can be clearly distinguished. The transition between  $H_1$  and  $L_\alpha$  is particularly sharp as

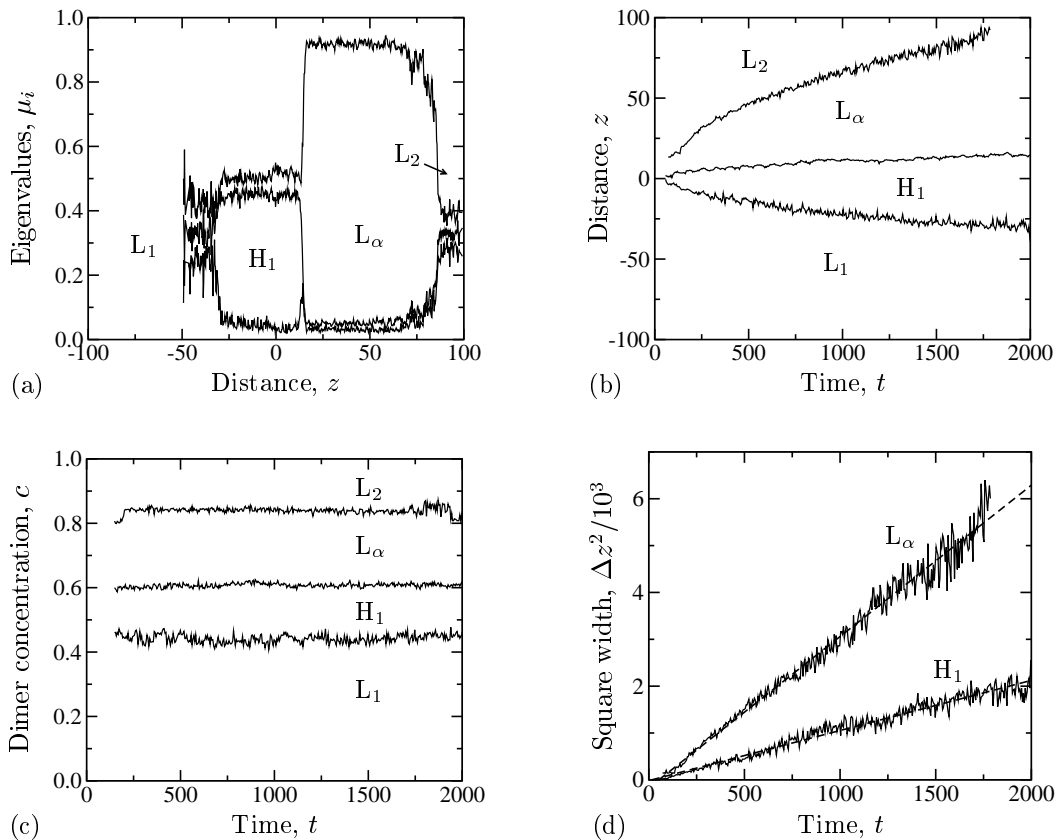


FIG. 2: (a) Eigenvalues of local order parameter tensor  $\mathbf{M}$  at  $t = 1200$  DPD time units after initial contact. (b) Phase boundary positions as a function of time, as determined from local order parameter tensor eigenvalues. (c) Local concentrations at phase boundaries as a function of time. (d) Squared widths of middle mesophases as a function of time.

can also be seen in Fig. 1(h). The above criteria are used to classify each slice and the positions of the boundaries between mesophases determined as a function of time. There is a short incubation period before the local order parameter can distinguish the different mesophases, but beyond this point, the boundaries can be reliably tracked as shown in Fig. 2(b). The key results are contained in Figs. 2(c) and (d), which show respectively the local composition at the mesophase boundary and the squared width of the middle two mesophases as a function of time.

Fig. 2(c) shows that the local compositions become established at constant values almost as soon as mesophases can be distinguished. Table II shows that the  $L_1$ - $H_1$  and  $H_1$ - $L_\alpha$  boundaries in the kinetic simulation lie almost exactly at the point expected from the equilibrium phase diagram. The  $L_\alpha$ - $L_2$  boundary is displaced from that found in the equilibrium phase diagram, but it is clear from Fig. 2(a) that this boundary is not completely sharp. Apart from this boundary therefore, it appears that the mesophases grow adiabatically almost from the earliest moments that the local order parameter can distinguish the growing mesophases.

TABLE II: Composition at mesophase boundaries from equilibrium  $k_B T = 1$  isotherm in Fig. 1(a), compared to those determined from kinetic simulation in Fig. 2(c). Units are dimer concentration  $c$  (the figure in brackets is an estimate of the error in the final digit).

Boundary	$L_1$ - $H_1$	$H_1$ - $L_\alpha$	$L_\alpha$ - $L_2$
Equilibrium	0.435(5)	0.605(5)	0.875(5)
Kinetic	0.44(1)	0.61(1)	0.84(1)

Fig. 2(d) shows that both mesophases follow a  $\Delta z^2 \propto t$  law, where  $\Delta z$  is the mesophase width. This is a classic verification of diffusion control. To further examine this, we fit the slope to what would be expected if the local composition followed a simple diffusion law:

$$\Delta z^2 = 4D[\text{erf}^{-1}(2c_2 - 1) - \text{erf}^{-1}(2c_1 - 1)]^2 t, \quad (1)$$

where  $D$  is an *effective* diffusion coefficient, and  $c_{1,2}$  are the fixed compositions at the edges of the mesophase of interest. The results are shown in Table III, where for comparison we have included the diffusion coefficients for the two pure components, ie dimers in a pure dimer fluid

TABLE III: Slope of  $\Delta z^2$  vs  $t$  plot from Fig. 2(d), and effective diffusion coefficient  $D$  determined from Eq. (1) for the two middle mesophases, compared to self diffusion coefficients for solvent particles and dimers in the pure components. Units are DPD units.

Mesophase	H <sub>1</sub>	L <sub>α</sub>	solvent	dimers
Slope	1.07(1)	3.23(2)		
Effective $D$	3.0(5)	3.2(4)	0.219(3)	0.092(2)

and solvent particles in pure solvent, determined from separate simulations. The effective diffusion coefficients are slightly different in the two phases, similar to the finding our previous experiments [3], although the difference here is within the statistical errors. Thus we conclude that, whilst the diffusion coefficient may be weakly composition- and mesophase-dependent, the whole process is diffusion controlled from the earliest times for which mesophases can be distinguished. Intriguingly the effective diffusion coefficients in the mesophases are considerably greater than the self diffusion coefficients in the pure components. This suggests the existence of a sizeable free energy driving force enhancing diffusion and is reminiscent of a detailed study on the H<sub>1</sub> phase of the C<sub>12</sub>E<sub>6</sub> / water system [12]. Note that the orientation of the H<sub>1</sub> and L<sub>α</sub> phases in the simulation is such that mutual diffusion occurs in the ‘easy’ direction: along the hexagonal rods, or parallel to the lamellar layers (we have also extracted orientation information from the eigenvectors of  $\mathbf{M}$  which will be reported elsewhere).

We can use the effective diffusion coefficients to map elapsed times in our mesoscale simulation onto real times. The corresponding diffusion coefficients in nonionic surfactant systems are typically  $2 \times 10^{-10} \text{ m}^2 \text{ s}^{-2}$  [3]. The lamellar repeat spacing  $L$  can be used as a common measure of length:  $L \approx 2.5$  DPD units in the simulation, and typically  $L \approx 5 \text{ nm}$  in real systems. By using  $L^2/D$  to scale time, we conclude one DPD time step is approximately equivalent to 50 ns. Thus the duration of the whole simulation (2000 DPD time units) represents more than 0.1 ms of real time, equivalent to  $10^8$  molecular dynamics time steps. Fig. 2 shows that adiabatic diffusion controlled dissolution sets in after about 200 DPD time units, equivalent to about  $10 \mu\text{s}$ , which is the origin of the time scale quoted in the introduction.

Our simulations, whilst addressing very directly intriguing questions concerning surfactant dissolution, are also interesting because they are simulations of phase formation kinetics starting from a highly inhomogeneous state rather than the usual approach which is to quench a homogeneous system. To our knowledge, the only com-

parable study in the past has been the disappearance of an interface in a vapour-liquid or binary liquid mixture after an ‘antiquench’ (sudden increase in temperature) [13]. It is indeed striking that we do *not* find any evidence of the delayed appearance of mesophases due to metastability, unlike that seen experimentally in temperature-jump experiments [14], nor do we find any systematic displacement of the mesophase boundaries by the strong concentration gradients present at such early times.

Our mesoscale model is also well suited to other fundamental (meso)phase studies such as temperature quenches [6, 14], the effect of shear on phase boundaries, the exploration of epitaxial relationships such as between the H<sub>1</sub> and L<sub>α</sub> phases in the present simulations, amongst many other possibilities.

- 
- [1] R. G. Laughlin, *Adv. Coll. Int. Sci.* **41**, 57 (1992).
  - [2] P. B. Warren and M. Buchanan, *Current Opin. Coll. Int. Sci.* **6**, 287 (2001).
  - [3] B. H. Chen, C. A. Miller, J. M. Walsh, P. B. Warren, J. N. Ruddock, P. R. Garrett, F. Argoul, and C. Leger, *Langmuir* **16**, 5276 (2000).
  - [4] R. G. Laughlin and R. L. Munyon, *J. Phys. Chem.* **91**, 2999 (1987).
  - [5] R. D. Groot and P. B. Warren, *J. Chem. Phys.* **107**, 4423 (1997).
  - [6] S. Jury, P. Bladon, M. Cates, S. Krishna, M. Hagen, J. N. Ruddock, and P. B. Warren, *Phys. Chem. Chem. Phys.* **1**, 2051 (1999).
  - [7] R. G. Laughlin, *The aqueous phase behaviour of surfactants* (Academic, New York, 1994).
  - [8] R. G. Larson, *J. Phys. II (France)* **6**, 1441 (1996). For a recent review see J. C. Shelley and M. Y. Shelley, *Current Opin. Coll. Int. Sci.* **5**, 101 (2000).
  - [9] K. V. Mardia, *Statistics of directional data* (Academic, New York, 1972).
  - [10] K. Michielsen and H. de Raedt, *PhysRep.* **347**, 461 (2001).
  - [11] This is easy to implement since isosurface normals are used in the lighting model to generate the images, and a representative sample can be extracted by intercepting the graphics pipeline. For visualisation purposes we use VTK : W. Schroeder, K. Martin and B. Lorensen, *The visualisation toolkit* (Prentice Hall, New Jersey, 1998). A similar order parameter could also be constructed directly from the dimer orientation distribution function.
  - [12] L. Sallen, P. Oswald, and P. Sotta, *J. Phys. II (France)* **7**, 107 (1997).
  - [13] W.-J. Ma, P. Keblinski, A. Maritan, J. Koplik, and J. R. Banavar, *Phys. Rev. Lett.* **71**, 3465 (1993).
  - [14] M. Clerc, P. Lagner, A.-M. Levelut, and G. Rapp, *J. Phys. II (France)* **5**, 901 (1995).